Title
Near-IR image-guided laser ablation of demineralization on tooth occlusal surfaces

Journal
Lasers in Surgery and Medicine, 48(1)

ISSN
0196-8092

Authors
Tom, Henry
Chan, Kenneth H
Darling, Cynthia L
et al.

Publication Date
2016

DOI
10.1002/lsm.22438

Peer reviewed

HHS Public Access

Author manuscript

Lasers Surg Med. Author manuscript; available in PMC 2016 March 04.

Published in final edited form as:

Lasers Surg Med. 2016 January ; 48(1): 52–61. doi:10.1002/lsm.22438.

Near-IR Image-Guided Laser Ablation of Demineralization on Tooth Occlusal Surfaces

Henry Tom, BA, **Kenneth H. Chan, BS**, **Cynthia L. Darling, PhD**, and **Daniel Fried, PhD***

Department of Preventive and Restorative Dental Science, University of California, San Francisco, California 94143-0758

Abstract

Introduction—Studies have shown that reflectance images at near-IR wavelengths coincident with higher water absorption are well-suited for image-guided laser ablation of carious lesions since the contrast between sound and demineralized enamel is extremely high and interference from stains is minimized. The objective of this study was to demonstrate that near-IR reflectance images taken at a wavelength range of 1,500–1,700 nm can be used to guide a 9.3 μm CO_2 laser for the selective ablation of early demineralization on tooth occlusal surfaces.

Methods—The occlusal surfaces of ten sound human molars were used in this in vitro study. Shallow simulated caries lesions with random patterns and varying depth and position were produced on tooth occlusal surfaces. Sequential near-IR reflectance images at 1,500–1,700 nm were used to guide the laser for the selective removal of the demineralized enamel. Digital microscopy and polarization sensitive optical coherence tomography (PS-OCT) were used to assess selectivity.

Results—Images taken before and after lesion removal suggest that the demineralized areas were removed with high selectivity. Although the estimated volume of tissue ablated was typically higher than the initial lesion volume measured with PS-OCT, the volume of enamel removed by the laser correlated well with the initial lesion volume.

Conclusion—Sequential near-IR reflectance images at 1,500–1,700 nm can be used to guide a 9.3 μm CO_2 laser for the selective ablation of early demineralization on tooth occlusal surfaces.

Keywords

selective laser ablation; image-guided ablation; carbon dioxide laser; near-IR imaging; optical coherence tomography

INTRODUCTION

In order to implement an image-guided approach for selectively removing carious lesions, images of demineralization on tooth surfaces will need to be acquired and subsequently used

*Correspondence to: Daniel Fried, PhD, Department of Preventive and Restorative Dental Sciences, University of California, San Francisco, 707 Parnassus Ave. CA 94143-0758. daniel.fried@ucsf.edu.

Conflict of Interest Disclosures: All authors have completed and submitted the ICMJE Form for Disclosure of Potential Conflicts of Interest and have disclosed the following: [None of the authors have potential conflicts of interest that need to be disclosed.]"

to guide a laser to selectively ablate those areas. This approach requires the rapid acquisition of high-contrast images of enamel and dentin demineralization that can be input into the laser-scanning system to selectively remove decay. Compact scanning and positioning is now feasible due to recent advances in compact high-speed laser scanning technology such as Micro-electro-mechanical systems (MEMS) mirrors and miniature galvanometer “galvo” based scanners. One approach is to remove the lesion layer by layer, that is, image the lesion then scan the laser beam over the lesion area, then re-image and scan again repeating that process until the lesion is completely removed.

Fluorescence has been combined with laser ablation for caries removal. Eberhard et al. [1–3] have combined laser ablation with an Er: YAG laser with red fluorescence (655 nm excitation, 680+ detection) and they claim this combination can be used to selectively remove infected dentin. Lennon and Buchalla et al. [4–6] have developed red fluorescence aided caries excavation (FACE) for use with the conventional handpiece and claim it has superior performance than conventional excavation, caries detector dyes and chemomechanical removal. They used 370 nm excitation and 530 nm+ detection. However, methods that employ red fluorescence for guidance are ineffective for the detection of surface demineralization that has minimal fluorescence from porphyrins.

Tao et al. [7] created patterned artificial lesions on blocks of bovine enamel and demonstrated that images of the patterned lesions acquired using near-IR transillumination measurements at 1,300 nm could be used to guide a 9.3 μm CO_2 laser for highly selective laser ablation. However, flat enamel blocks were used for that study and near-IR transillumination is poorly suited for acquiring high contrast images of shallow demineralization on tooth occlusal surfaces due to the large volume of tooth structure that has to be imaged through on whole teeth.

Recent studies suggest that near-IR reflectance imaging is ideally suited for acquiring high-contrast images for image guided ablation due to the weak light scattering from sound enamel and the lack of interference from stain [8–10]. Stains that greatly interfere with visible reflectance and fluorescence based measurements of lesion contrast, do not interfere at near-IR wavelengths. Stains cause the lesion areas to appear darker, not lighter, in the visible range, and the stained areas do not represent the areas of demineralization. This is why visible reflectance measurements are of limited effectiveness on occlusal surfaces [11,12] and are not suitable for guiding laser ablation. In addition, the near-IR has high transmission through zinc selenide optics which is an important advantage when working with CO_2 lasers. A comparison of Quantitative light fluorescence (QLF), near-IR (1,310 nm) and visible cross-polarization reflectance imaging for early demineralization, indicated that the highest lesion contrast was for near-IR reflectance [13]. Cross-polarization imaging is useful for removing the strong specular reflection “glare” from sound surfaces during reflected light imaging. More recent reflectance measurements at 1,460 nm and 1,500–1,700 nm yielded even higher contrast than other near-IR wavelengths because the peak in water absorption at this wavelength reduces the intensity of back scattered light from the underlying dentin [14,15]. Near-IR measurements also manifest a greater range in contrast values correlating with increased severity of demineralization and the near-IR can better represent variations in lesion severity [16].

A potential concern is that thermal modification and roughening of the surface by the laser may interfere with the ability to acquire useful images of previously irradiated surfaces. The reduction in contrast between sound and demineralized enamel was measured after surface modification by a carbon dioxide laser for visible and near-IR reflectance, and QLF by LaMantia et al. [17]. Lesion contrast was significantly higher (P <0.05) for near-IR reflectance versus visible reflectance and fluorescence both before and after laser irradiation. After laser modification of the enamel surface the mean contrast values were reduced by 67% for fluorescence, 28% for visible reflectance, and the contrast values increased by 1% for the near-IR. The significant reduction in the contrast for QLF suggests that it is not well-suited for image guided ablation. The greatest contrast was attained at 1,460 nm and 1,500–1,700 nm, wavelengths coincident with higher water absorption. The reflectance did not decrease significantly after laser irradiation for those near-IR wavelengths. However, water on the tooth surface is a concern and it is likely that images will have to be acquired while the surfaces are dry. This can be easily accomplished with a pulsed air/water cooling system that is already used for hard tissue laser ablation systems. Recent studies suggest that near-IR reflectance imaging at 1,500–1,700 nm is highly promising for the serial removal of demineralization from tooth occlusal surfaces [18,19]. However, those studies were limited to the visual assessment of a few examples and lack a comprehensive assessment of ablation selectivity.

The objective of this study was to demonstrate that near-IR reflectance images taken at a wavelength range of 1,500–1,700 nm could be used to guide a CO_2 laser (λ = 9.3 μm) for the selective ablation of early demineralization on tooth occlusal surfaces. This was achieved by comparing the initial volume of demineralization with the volume selectively removed by the laser using polarization sensitive optical coherence tomography (PS-OCT) [18–20].

MATERIALS AND METHODS

Sample Preparation

Ten human teeth without visible demineralization on the occlusal surfaces were collected (Exempt, IRB not required) and sterilized with gamma radiation. All teeth were mounted in black orthodontic acrylic blocks. Samples were stored in a moist environment of 0.1% thymol to maintain tissue hydration and prevent bacterial growth. Tooth occlusal surfaces were cleaned/polished with a prophyl angle with pumice paste to ensure a homogeneous surface for demineralization. The outlines of 4 × 4 mm windows approximately 50 μm deep were cut on the occlusal surface of each tooth using a CO_2 laser (Impact 2500, GSI Lumonics, Rugby, United Kingdom) around the suspected lesion area as shown in Figure 1. The channels cut by the laser serve as reference points for imaging and serial sectioning and are sufficiently narrow that they do not interfere with calculations of the image contrast. The enamel surrounding the 4 × 4 mm windows created by the laser was covered with a red acid-resistant varnish (Revlon, New York). Clear nail polish was dabbed randomly inside the 4 × 4 mm windows to generate random patterns for the artificial lesions. Artificial lesions were created within the 4 × 4 windows by immersing each tooth into a 50 ml aliquot of a Ca/PO_4/acetate solution containing 2.0 mmol/L calcium, 2.0 mmol/L phosphate, and 0.075 mol/L

acetate maintained at pH 4.5 and a temperature of 37°C for 3-days [21]. After the last day of demineralization, the acid resistant varnish was removed with acetone. Lesion presence was verified using PS-OCT and the mean lesion depth was approximately 150 μm.

Laser System

Samples were irradiated using an industrial marking laser, Impact 2500 from GSI Lumonics operating at a wavelength of 9.3 μm using the setup shown in Figure 2. The laser was custom modified to produce a Gaussian output beam (single spatial mode) and a pulse duration between 10 and 15 μs. The laser energy output was monitored using a power meter EPM 1000, Coherent-Molectron (Santa Clara, CA), and the Joulemeter ED-200 from Gentec (Quebec, Canada). Computer-controlled XY galvanometers 6200HM series with MicroMax Series 671 from Cambridge Technology, Inc. (Cambridge, MA) were used to scan the laser beam over the sample surfaces. An air-actuated fluid spray delivery system consisting of a 780S spray valve, a Valvemate 7040 controller, and a fluid reservoir from EFD, Inc. (East Providence, RI) was used to provide a uniform spray of fine water mist onto the tooth surfaces at 2 ml/min. The reference boxes were cut into the samples using a spot size of 200 μm, an overlap of 50 μm and a pulse repetition rate of 50 Hz with 30 mJ per pulse.

Near-IR Cross Polarization Reflectance Images

In order to acquire reflected light images, near-IR light was directed towards the occlusal surface of each sample. Crossed polarizers were placed after the light source and before the detector and used to remove specular reflection (glare) that interferes with measurements of the lesion contrast. The near-IR reflectance images were captured using a 320 × 240 element InGaAs area camera SU320-KTSX from Sensors Unlimited (Princeton, NJ) sensitive from 900 to 1,700 nm with a 25 μm pixel pitch. Reflectance measurements were taken in the wavelength range of 1,500–1,700 nm using a 1,500 nm long-pass filter, FEL 1,500 from Thorlabs (Newton, NJ).

Near-IR Guidance (Description of Procedures Flowchart)

The CO_2 laser was guided by near-IR reflectance images of the samples. The flowchart shown in Figure 3 shows the procedure employed during the removal process. An initial near-IR background image was acquired that was used for illumination non-uniformity correction. Each sample was then placed on a magnetic sample holder (Model KB1 × 1, Thorlabs) that could be switched back and forth between magnetic mounts on the laser and imaging setups. The initial background image was subtracted from each subsequent image acquired. Maximum pixel intensity values in the 4 × 4 mm Region of interest (ROI) (83 × 83 pixels) and average sound values from outside the ROI were calculated from the first corrected image and used for subsequent assessments of the post ablation images. The image/lesion contrast was calculated for each pixel in the ROI using $(I_{ROI} - I_{MS})/I_{ROI}$ where I_{MS} is the mean intensity of the sound enamel pixels outside the ROI and I_{ROI} is the value of the individual pixels in the ROI to yield values between 0 and 1. A threshold demarcating the lesion area in the ROI was manually selected after comparing the near-IR images acquired before and after generation of the artificial lesions. Once the threshold was selected, the ROI image was then converted to a binary look-up table (LUT). The look-up

table (LUT) was used to direct the laser beam to ablate matched areas on the sample as can be seen in Figure 1B.

The laser was operated at a pulse repetition rate of 100 Hz and the beam was focused to a spot size of ~350 μm using a ZnSe scanning lens of 90 mm focal length for an incident fluence of 20 J/cm^2 (19 mJ per pulse). The beam was scanned from point to point in 100 μm increments with four laser pulses per position. All designated areas of demineralization were irradiated during each iteration (scan) and new near-IR images were acquired after every two iterations. This process was repeated until a final near-IR image indicated that all demineralized areas were removed.

PS-OCT System

An all-fiber-based optical coherence domain reflectometry (OCDR) system (time-domain) with polarization maintaining (PM) optical fiber, high-speed piezoelectric fiber-stretchers, and two balanced InGaAs receivers that was designed and fabricated by Optiphase, Inc., (Van Nuys, CA) was used. This two-channel system was integrated with a broadband superluminescent diode (SLD) Denselight (Jessup, MD) and a high-speed XY-scanning system (ESP 300 controller and 850G-HS stages, National Instruments, Austin, TX) for *in vitro* optical coherence tomography. This system is based on a polarization-sensitive Michelson white light interferometer. The high power (15 mW) polarized SLD source operated at a center wavelength of 1,317 nm with a spectral bandwidth full-width at half-maximum (FWHM) of 84 nm. The sample arm was coupled to an AR-coated fiber-collimator to produce a 6 mm diameter, collimated beam. That beam was focused onto the sample surface using a 20 mm focal length AR-coated planoconvex lens. This configuration provided lateral resolution of approximately 20 μm and an axial resolution of 10 μm in air with a signal to noise ratio of greater than 40–50 dB. The PS-OCT system is completely controlled using Labview software (National Instruments). The system is described in greater detail in the following reference [22]. Acquired scans are compiled into b-scan [23] image files. Image processing was carried out using Igor Pro, data analysis software (Wave-metrics Inc., Lake Oswego, OR). PS-OCT images consisted of two orthogonal images, a co-polarization image with the same polarization as the incident light and a cross-polarization image with the orthogonal polarization. The cross-polarization OCT image (CP-OCT) was used to assess the depth of demineralization.

Digital Microscopy

Tooth surfaces were examined after laser irradiation using an optical microscopy/3D surface profilometry system, the VHX-1000 from Keyence (Elmwood, NJ). The VH-Z25 lens with a magnification from 25 to 175× was used. Depth composition digital microscopy images (DCDM) were acquired by capturing serial images of varying depth and reconstructing a depth composition image with all points at optimum focus displayed in a 2D image. Images of the samples were acquired before and after ablation at 25× and 50× magnification. The Keyence 3-D shape measurement software, VHXH3M, was used to correct the tilt of the sample and measure the variation in the surface topography of tooth occlusal surfaces.

Polarized Light Microscopy

After sample imaging was completed, approximately 200 μm thick serial sections were cut using an Isomet 5000 saw (Buehler, IL), for polarized light microscopy (PLM). PLM was carried out using a Meiji Techno RZT microscope (Meiji Techno Co., LTD, Saitama, Japan) with an integrated digital camera, Canon EOS Digital Rebel XT (Canon Inc., Tokyo, Japan). The sample sections were imbibed in water and examined in the bright field mode with crossed polarizers and a red I plate with 500 nm retardation.

Analysis of Selectivity and Lesion Volume Assessment

Images were acquired before and after artificial lesion removal using digital microscopy (DCDM) and PS-OCT. Images were then compared to their respective cross-polarization OCT (CP-OCT) images to confirm the existence of artificial lesions. Teeth were sectioned after treatment and the 200 μm thick sections were examined using polarized light microscopy (PLM).

Two methods were used to assess the volume of demineralization in the region of interest, that is, the volume to be ablated. In the first method, the demineralized tissue volume was measured using the CP-OCT images. An automated program written in Labview employing edge detection was used to calculate the lesion depth from each a-scan [23] and from that determine the initial lesion volume. In the second method the cross-polarization images were converted into TIF images through Matlab (Mathworks, Natick, MA),which were then loaded into Avizo (FEI Software, Hillsboro, OR). Avizo is a 3D analysis program for scientific data. Orthogonal slices in the yz-plane were created providing a top-down progression of images through the occlusal surface. The range of slices from each cross-polarization image containing demineralized enamel was manually determined on the basis of increased reflectivity from demineralized areas. A built in edge detection function in Avizo using Canny edge thresholding [24] was applied to each slice in this range to determine the area of demineralization for each slice. The yz slices were combined to yield the lesion volume. The volume of tissue removed by laser was estimated using look-up tables for the rate of ablation at an incident fluence of 20 J/cm^2. The volume ablated was determined by summing the look-up table values together with a correction factor added to account for the overlap of laser pulses. Linear regression was carried out using Prism (Graphpad Software, La Jolla, CA).

For one sample, sample three, the lesion was not detected using the automated lesion assessment program in Labview and the initial lesion volume was recorded as 0. Since no pre-ablation volume was available for comparison, this sample was rejected and not used in the fit for comparison with automated assessment. However, it was included in the initial manual lesion volume assessment carried out using Avizo.

RESULTS

PS-OCT images were compared before and after ablation to assess the selectivity of the artificial lesion removal process. These images represent cross sections of the tooth samples and indicate the initial lesion depth and the depth of ablation. The PS-OCT images clearly

show the removal of artificial lesions; however, there are still areas with higher “residual” reflectivity caused by the increased surface roughness produced by laser irradiation. Images from two of the tooth samples are shown in Figures 4 and 5.

Cross-polarization OCT b-scans across the sample at the positions indicated by the yellow dotted lines in A–D are shown in E and F. The yellow arrows in all images indicate the beginning and end of the ROI window corresponding to the OCT images. Images A and B are DCDM images and C and D are near-IR reflectance images before and after removal. In C, the artificial lesions have high contrast as indicated by the white patches, while D shows that the artificial lesions were removed within the area of the box. From the left yellow arrow to the right arrow, artificial lesions are present along the surface of the scan as indicated by the higher reflectivity in E. After ablation, the artificial lesions have disappeared as indicated by the rough surface in F.

DCDM images before and after the laser scans are shown in Figure 6 for samples seven and eight and they clearly show that the majority of artificial lesions were removed. As can be seen in A and B most of the whiter areas (higher reflectivity) indicative of demineralization have been removed after scanning.

Serial imaging during the ablation process is shown in Figure 7 for sample eight. Each image was acquired after the laser was scanned over the targeted area twice. As shown, the areas of higher reflectivity gradually disappears as each iterative step progresses until the lesion is removed. As previously mentioned, some surface roughening is visible which is evident after the last iteration (10 scans). Avizo was used to generate 3D surface renderings from the OCT data as shown in Figure 8 for the same sample. Both the DCDM and Avizo images match quite closely. Avizo was also used to process the OCT volumetric data to determine the lesion volume as shown in Figure 8. The black cross section on the right can be seen in its corresponding position on the tooth surface on the left. Bright white areas in the cross section indicated by the arrow represent the amount removed by the laser.

A plot of the initial lesion volume assessed manually using Avizo is shown in Figure 9 versus the volume removed by the laser for the ten samples. There was a significant positive correlation (P <0.05) of the initial lesion volume, $R^2 = 0.57$, $n = 10$, although the volume removed was typically less than the lesion volume initially present. A similar plot using the initial lesion volume assessed using the automated Labview program (minus sample three) also yielded a significant positive correlation with the volume removed, P <0.05, $R^2 = 0.50$, $n = 9$. The initial lesion volume calculated from the CP-OCT images was similar for the two methods, manual (Avizo) versus automated (Labview program), showing a high positive correlation of $R^2 = 0.86$, $n = 9$ (minus sample three).

The rendered 3D surface in Avizo for sample seven is shown in Figure 10 with corresponding OCT b-scan images extracted at the same position before and after lesion removal. The area removed by the laser can be seen in the overlay of the two OCT b-scan images between the red lines shown in Figure 10B.

DISCUSSION

It was anticipated that the volume removed should be larger than the initial lesion volume. However, the plot in Figure 9 suggests that the volume ablated exceeded the initial lesion volume by almost a factor of two. This is most likely due to the use of the ablation rate of sound enamel for estimation of the ablation depth, the ablation rate of demineralized enamel is much higher. However, since the mean lesion depth for the artificial lesions is ~150 μm, the difference in the ablated depth is well under 100 μm. Even with the higher ablation depths the selectivity of ablation in the highly convoluted topography of the occlusal surface is impressive and obviously far exceeds what would be achievable with the dental drill.

There was still some residual contrast visible even though the lesions were completely removed as can be seen in Figures 4–6. As previously mentioned, the higher reflectivity in irradiated areas is due to increased surface roughness due to the laser and is not residual demineralization [17]. In our study presented last year, we evaluated the effects of the CO_2 laser modified surfaces on the contrast in NIR reflectance. There were changes but they did not reduce the contrast to the degree that NIR reflectance was unsuitable for serial imaging during ablation [17]. The increase in reflectivity caused by surface modification/roughening manifests itself in all of the imaging modalities, NIR reflectance, visible reflectance and OCT and presents a challenge in automating the caries removal process.

Even though magnetic sample holders were used, there were some alignment problems with switching between the laser irradiation and near-IR imaging setups. For example, sample seven, had some minor error due to accidental movement of the sample placeholder towards the end of the data collection. In addition, sample one also had issues with alignment, leaving a small fraction of the 4 × 4 mm window out of the ROI. In sample two, (see Fig. 6) deviation from the rest of the data can be attributed to multiple iterations to ablate one specific area, consequently ablating more of the surrounding area along with it. A secondary goal of this study was to demonstrate that PS-OCT could be used to both assess the lesion depth and severity before ablation and subsequently measure the volume of tissue ablated. We used two different methods to assess the initial lesion volume, a manual method based on contrast thresholding in which Avizo was used to examine the CP-OCT images slice by slice and a more automated method in which a program written in Labview was used to calculate the lesion depth for each a-scan based on a $1/e^2$ intensity threshold for base of the lesion. Both methods agreed quite well with the exception that the automated labview program failed to detect the lesion for sample three. The automated approach for lesion assessment (Labview program) was used in previous studies [25–27]. However, accurate calculation of the lesion depth from OCT images is difficult because lesions do not have sharp boundaries and the reflectivity varies markedly throughout the breadth of the lesion. Moreover, biological variation in refractive index (RI) with mineral content and composition, and optical dispersion (variation of RI with wavelength) can all influence the lesion depth calculations for OCT. We have experimented with various approaches to set the cutoff (interior edge of lesion) including calibration against PLM histology [25] which is unique to each OCT system.

We had intended to use OCT to assess the volume of enamel ablated and then directly compare the initial lesion volume assessed with CP-OCT to the volume ablated measured with OCT. However, image registration was extremely difficult and even with the magnetic mounts it was not possible to achieve a good match of the initial surfaces for a majority of the samples for the before and after OCT images and the errors were too large for such shallow lesions. It is likely that this approach will be more successful for deeper lesions.

In the future, we plan to explore methods for image registration to improve the performance of OCT in monitoring the selectivity of ablation. In addition, we will directly integrate an InGaAs near-IR imaging camera with the laser ablation system so that the samples will not have to be repositioned during the removal process. After these modifications, we plan to repeat this study on natural occlusal lesions.

Ultimately it is desirable to fully automate the caries removal process by developing methods for image analysis that are capable of accurately identifying the appropriate contrast thresholds in the near-IR images as opposed to having the operator manually set thresholds as was done in this study. For a practical clinical image-guided ablation system, the clinician would need to review and approve the area designated by the computer before removal. An automated approach is more important for determination of the end point of removal, that is, accurately identifying when caries removal is complete. In addition to eliminating the noise and vibration associated with the dental hand-piece, lasers offer several unique advantages over current surgical technology for conservative dentistry. An integrated imaging system capable of both identifying areas of demineralization on tooth occlusal surfaces without the interference of stains should enable the precise and selective removal of decay with minimal loss of healthy tissues. Under the appropriate irradiation conditions, pulsed CO_2 lasers can induce beneficial chemical and morphological changes in the walls of the drilled cavity that can increase resistance to further dental decay [28–30]. In addition, such laser systems are ideally suited for remote operation.

In conclusion, the correlation between the volume of demineralization (lesion) present and the volume removed shows a clear positive trend, demonstrating the potential of near-IR reflectance measurements at 1,500–1,700 nm for guiding the CO_2 laser. This study demonstrates that high contrast near-IR reflectance images are suitable for the serial removal of demineralization on tooth occlusal surfaces through image-guided laser ablation with a pulsed CO_2 laser operating at 9.3 μm.

Acknowledgments

Contract grant sponsor: NIH/NIDCR; Contract grant numbers: R01-DE19631, R01-DE17869, R01DE14698.

This work was supported by NIH/NIDCR Grants R01-DE14698, R01-DE19631 and R01-DE17869. The authors would also like to thank Daniel Saltiel and Robert Lee for their contributions.

References

1. Eberhard J, Bode K, Hedderich J, Jepsen S. Cavity size difference after caries removal by a fluorescence-controlled Er: YAG laser and by conventional bur treatment. Clin Oral Investig. 2008; 12(4):311–318.

2. Eberhard J, Eisenbeiss AK, Braun A, Hedderich J, Jepsen S. Evaluation of selective caries removal by a fluorescence feedback-controlled Er: YAG laser in vitro. Caries Res. 2005; 39(6):496–504. [PubMed: 16251795]
3. Jepsen S, Acil Y, Peschel T, Kargas K, Eberhard J. Biochemical and morphological analysis of dentin following selective caries removal with a fluorescence-controlled Er: YAG laser. Lasers Surg Med. 2008; 40(5):350–357. [PubMed: 18563782]
4. Lennon AM. Fluorescence-aided caries excavation (FACE) compared to conventional method. Oper Dent. 2003; 28(4):341–345. [PubMed: 12877417]
5. Lennon AM, Attin T, Buchalla W. Quantity of remaining bacteria and cavity size after excavation with FACE, caries detector dye and conventional excavation in vitro. Oper Dent. 2007; 32(3):236–241. [PubMed: 17555174]
6. Lennon AM, Attin T, Martens S, Buchalla W. Fluorescence-aided caries excavation (FACE), caries detector, and conventional caries excavation in primary teeth. Pediatr Dent. 2009; 31(4):316–319. [PubMed: 19722440]
7. Tao YC, Fried D. Near-infrared image-guided laser ablation of dental decay. J Biomed Optics. 2009; 14(5):054045.
8. Bühler CM, Ngaotheppitak P, Fried D. Imaging of occlusal dental caries (decay) with near-IR light at 1310-nm. Opt Express. 2005; 13(2):573–582. [PubMed: 19488387]
9. Jones G, Jones RS, Fried D. Transillumination of inter-proximal caries lesions with 830-nm light. Lasers in Dentistry X; 2004. Proc SPIE Int Soc Opt Eng. 2004; 5313:17–22.
10. Jones RS, Huynh GD, Jones GC, Fried D. Near-IR Trans illumination at 1310-nm for the imaging of early dental caries. Opt Express. 2003; 11(18):2259–2265. [PubMed: 19466117]
11. Borsboom PCF, ten Bosch JJ. Fiber-optic scattering monitor for use with bulk opaque material. Appl Opt. 1982; 21(19):3531–3535. [PubMed: 20396271]
12. ten Bosch JJ, van der Mei HC, Borsboom PCF. Optical monitor of in vitro caries. Caries Res. 1984; 18:540–547. [PubMed: 6593126]
13. Wu J, Fried D. High contrast near-infrared polarized reflectance images of demineralization on tooth buccal and occlusal surfaces at λ = 1310-nm. Lasers Surg Med. 2009; 41(3):208–213. [PubMed: 19291753]
14. Chung S, Fried D, Staninec M, Darling CL. Multispectral near-IR reflectance and transillumination imaging of teeth. Biomed Opt Express. 2011; 2(10):2804–2814. [PubMed: 22025986]
15. Fried WA, Darling CL, Chan K, Fried D. High contrast reflectance imaging of simulated lesions on tooth occlusal surfaces at near-IR wavelengths. Lasers Surg Med. 2013; 45:533–541. [PubMed: 23857066]
16. Simon JC, Chan KH, Darling CL, Fried D. Multispectral near-IR reflectance imaging of simulated early occlusal lesions: Variation of lesion contrast with lesion depth and severity. Lasers Surg Med. 2014; 46(3):203–215. [PubMed: 24375543]
17. Lamantia NR, Tom H, Chan KH, Simon JC, Darling CL, Fried D. High contrast optical imaging methods for image guided laser ablation of dental caries lesions. Lasers in Dentistry XX 2014 Proc SPIE Int Soc Opt Eng. 2014; 8929:P1–P7.
18. Chan KH, Tom H, Darling CL, Fried D. Serial removal of caries lesions from tooth occlusal surfaces using near-IR image-guided IR laser ablation. Lasers in Dentistry XXI 2015 Proc SPIE Int Soc Opt Eng. 2015; 9306:G1–G6.
19. Tom H, Chan KH, Saltiel D, Fried D. Selective removal of demineralized enamel using a CO laser coupled with near-IR reflectance imaging. Lasers in Dentistry XXI 2015 Proc SPIE Int Soc Opt Eng. 2015; 9306:M1–M7.
20. Bush J, Davis P, Marcus MA. All-fiber optic coherence domain interferometric techniques. Fiber Optic Sensor Technology II 2000. Proc SPIE Int Soc Opt Eng. 2000; 4204:71–80.
21. Featherstone JDB, Glena R, Shariati M, Shields CP. Dependence of in vitro demineralization and remineralization of dental enamel on fluoride concentration. J Dent Res. 1990; 69:620–625. [PubMed: 2312892]
22. Fried D, Xie J, Shafi S, Featherstone JDB, Breunig T, Lee CQ. Early detection of dental caries and lesion progression with polarization sensitive optical coherence tomography. J Biomed Optics. 2002; 7(4):618–627.

23. Brezinski, M. Optical coherence tomography: Principles and applications. London: Elsevier; 2006.
24. Canny J. A computational approach to edge detection. IEEE Trans Pattern Anal Mach Intellig. 1986; PAMI-8(6):679–698.
25. Chan KH, Chan AC, Fried WA, Simon JC, Darling CL, Fried D. Use of 2D images of depth and integrated reflectivity to represent the severity of demineralization in cross-polarization optical coherence tomography. J Biophotonics. 2015; 8(1–2):36–45. [PubMed: 24307350]
26. Nee A, Chan K, Kang H, Staninec M, Darling CL, Fried D. Longitudinal monitoring of demineralization peripheral to orthodontic brackets using cross polarization optical coherence tomography. J Dent. 2014; 42(5):547–555. [PubMed: 24561340]
27. Lee RC, Kang H, Darling CL, Fried D. Automated assessment of the remineralization of artificial enamel lesions with polarization-sensitive optical coherence tomography. Biomed Opt Express. 2014; 5(9):2950–2962. [PubMed: 25401009]
28. Featherstone JDB, Nelson DGA. Laser effects on dental hard tissue. Adv Dent Res. 1987; 1(1):21–26. [PubMed: 3125842]
29. Fried D, Murray MW, Featherstone JDB, Akrivou M, Dickenson KM, Duhn C. Dental hard tissue modification and removal using sealed TEA lasers operating at λ = 9. 6 μm. J Biomed Opt. 2001; 6(2):231–238. [PubMed: 11375734]
30. Can AM, Darling CL, Ho C, Fried D. Non-destructive assessment of inhibition of demineralization in dental enamel irradiated by a λ = 9. 3-μm CO2 laser at ablative irradiation intensities with PS-OCT Lasers. Surg Med. 2008; 40(5):342–349.

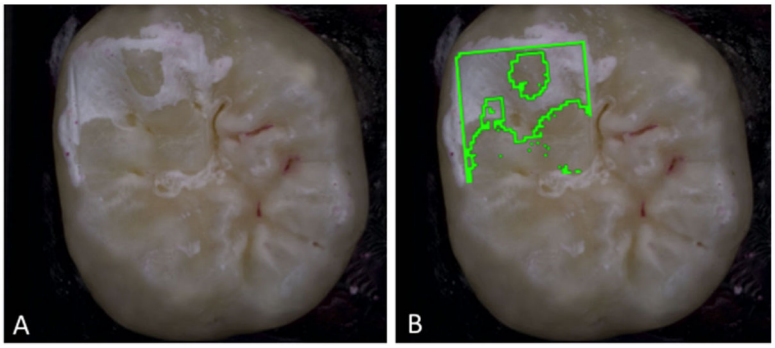

Fig. 1.

Digital microscope images (DCDM) of a tooth sample after exposure to the 72 hour demineralization solution (**A**). Demineralized areas are whiter due to increased reflectivity and light scattering. In (**B**) the outlined areas in green (LUT maps) are the areas designated for laser ablation from the near-IR reflectance images.

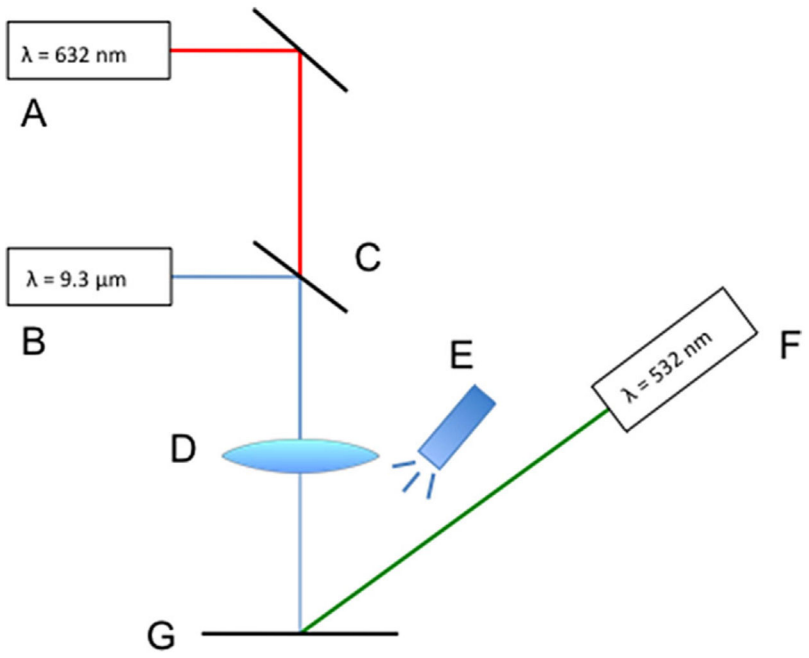

Fig. 2.

Experimental setup with a red diode laser (**A**), CO_2 laser (**B**), galvanometer (**C**), ZnSe f-theta scanning lens (**D**), water spray (**E**), Nd:YVO_4 green laser (**F**), and the sample (**G**).

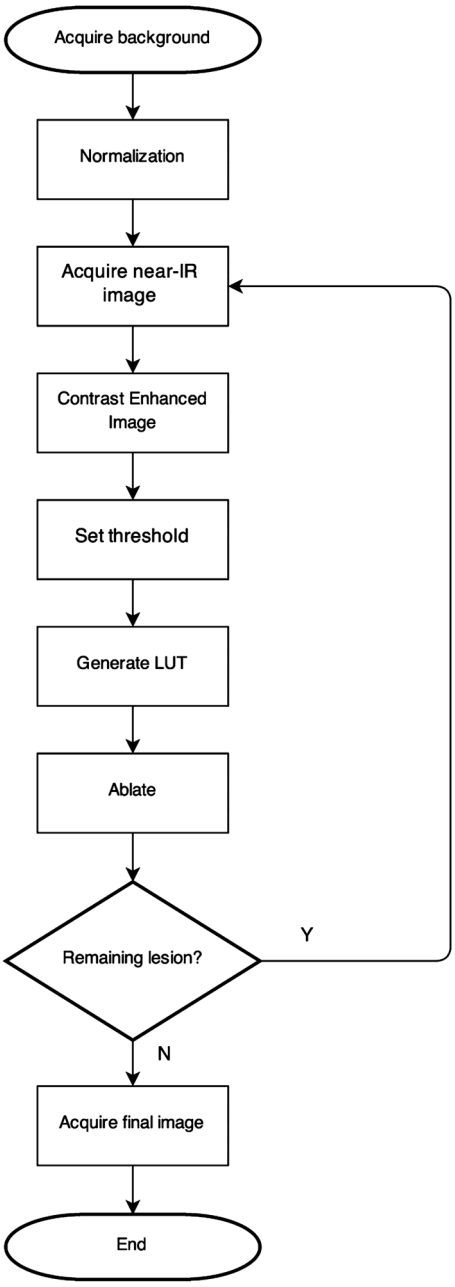

Fig. 3.
Flow-chart of experimental procedures.

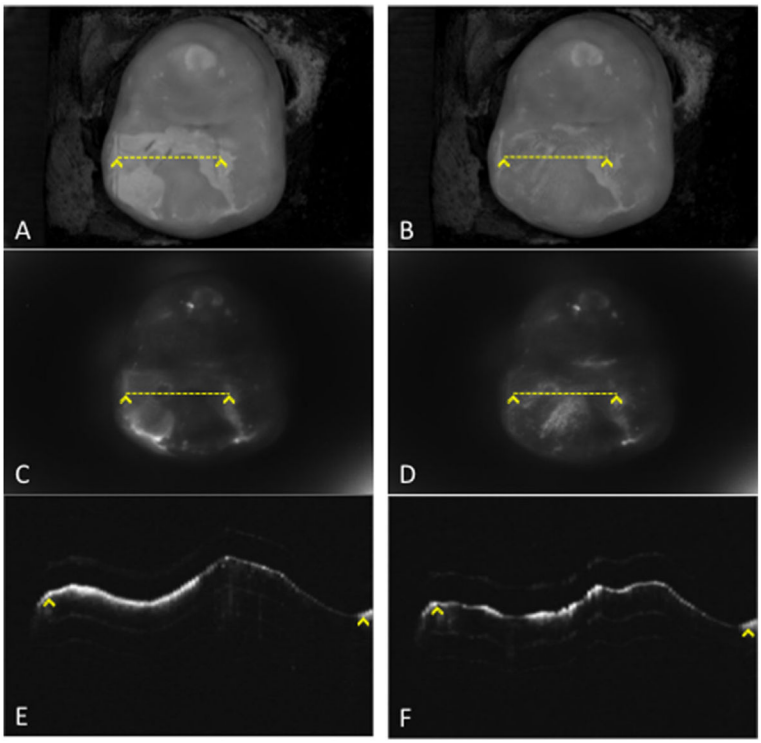

Fig. 4.

DCDM images of sample seven before (**A**) and after (**B**) removal, NIR reflectance images before (**C**) and after (**D**) removal, and corresponding CP-OCT cross sectional images (B-scans) before (**E**) and after (**F**) removal. The yellow dotted lines indicate the position of the CP-OCT B-scans on the tooth occlusal surface, while the yellow arrows indicate the beginning and end of the scan from left to right.

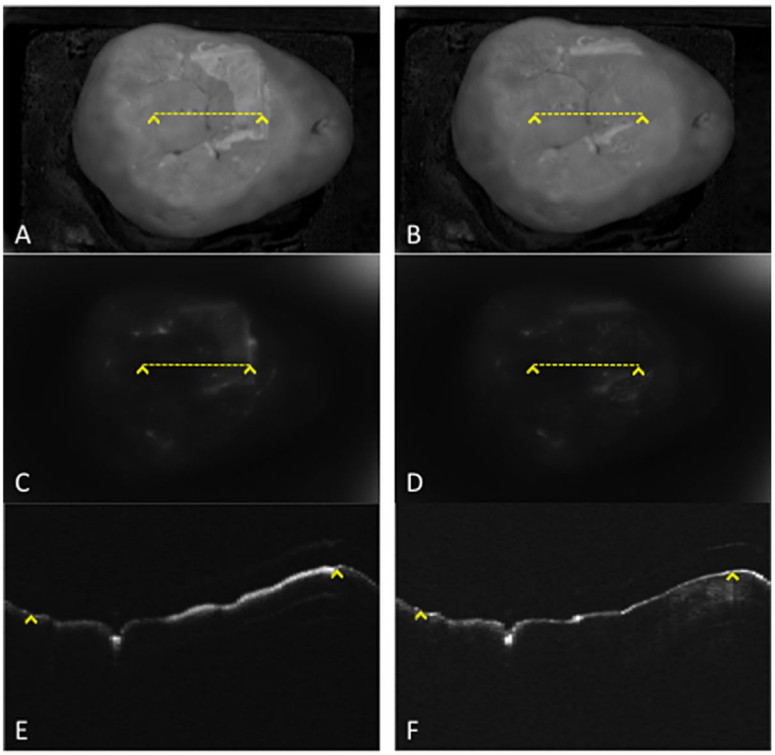

Fig. 5.

DCDM images of sample eight before (**A**) and after (**B**) removal, NIR reflectance images before (**C**) and after (**D**) removal, and corresponding CP-OCT cross sectional images (B-scans) before (**E**) and after (**F**) removal. The yellow dotted lines indicate the position of the CP-OCT B-scans on the tooth surface, while the yellow arrows indicate the beginning and end of the scan from left to right.

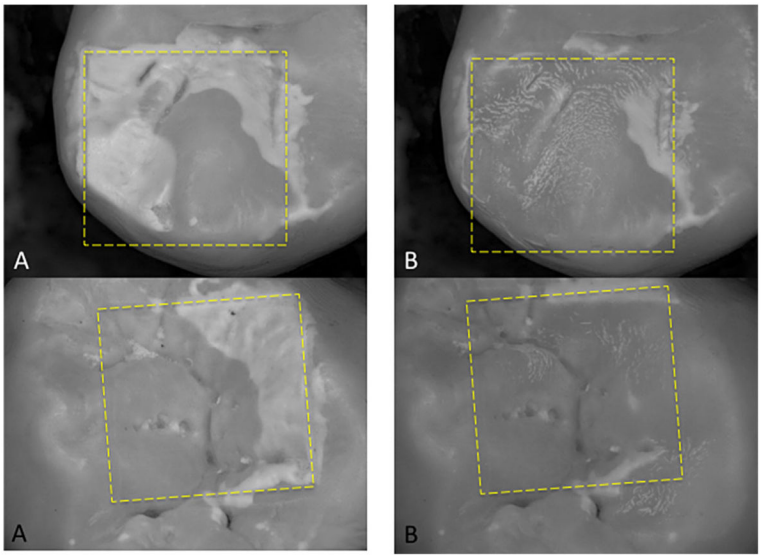

Fig. 6.

DCDM images acquired prior to (**A**) and after (**B**) removal for samples seven (top row) and eight (bottom row) at 50× magnification. The white areas in the images acquired prior to removal are the artificial lesion areas. Images after removal show that the artificial lesions within the 4 × 4 mm window have been removed, leaving sound enamel underneath.

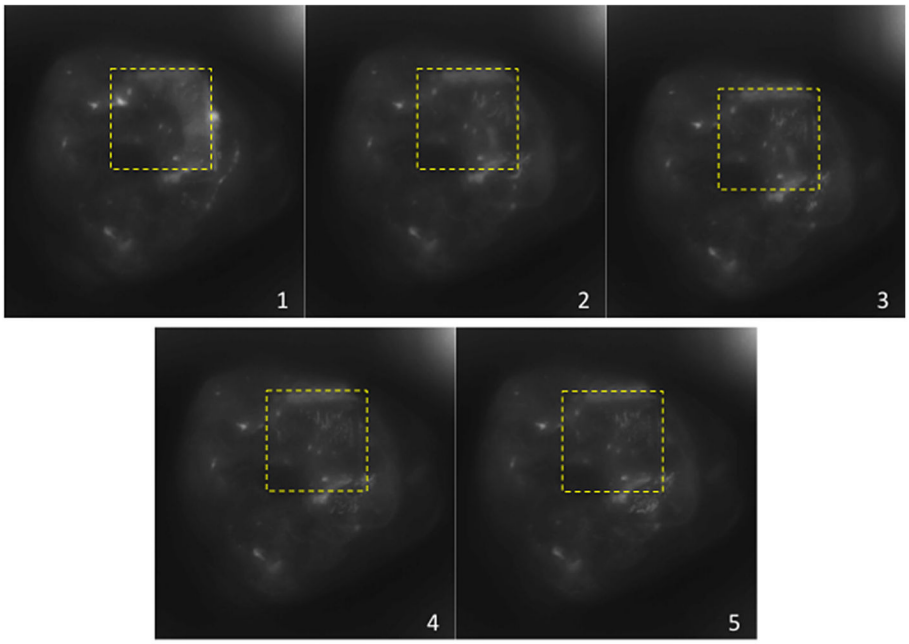

Fig. 7.

Sequential near-IR images acquired during the serial ablation of demineralization from one of the samples. The first image represents the initial image acquired prior to ablation. The areas of demineralization are removed with increasing number of iterations as shown in subsequent images.

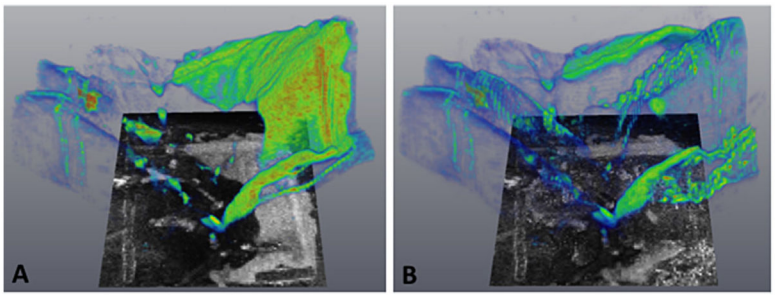

Fig. 8.

3D images rendered in Avizo for sample eight before (**A**) and after (**B**) lesion removal. The rendered images clearly show the white lesion present on the right half of the 4 × 4 mm window before selective removal and the lesion absent in the corresponding after image. Highly reflective lesions areas are shown in red and yellow.

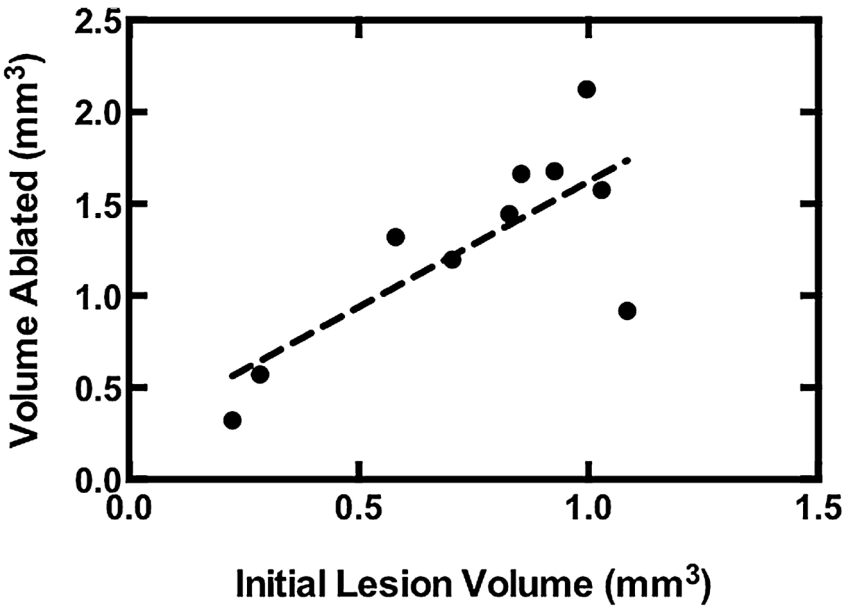

Fig. 9.

Plot of the volume removed (mm^3) versus the volume of lesion initially present (mm^3) determined from volumetric CP-OCT scans taken before and after lesion removal for 10 samples.

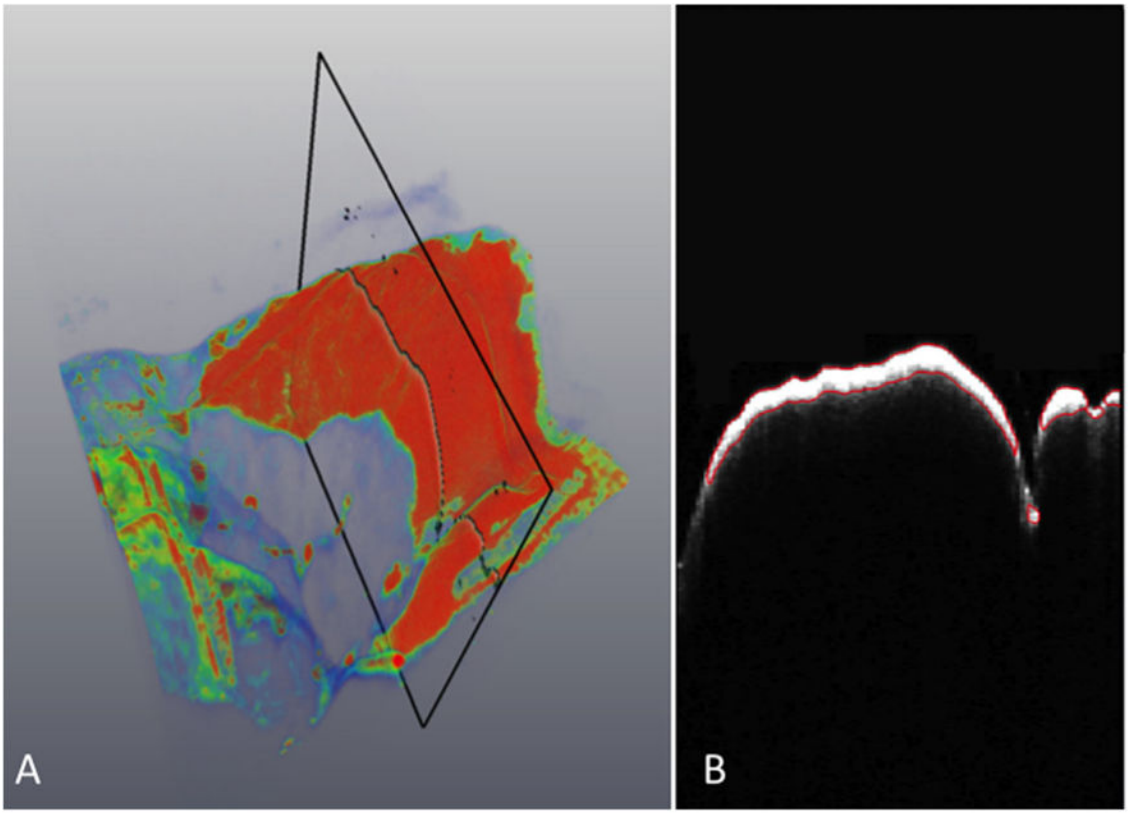

Fig. 10.

Rendered 3D surface in Avizo for sample seven (**A**) with corresponding OCT b-scan image (**B**), extracted at the position shown in the black box of (A) highlighting the region removed by the laser. The area removed by the laser is in white and located between the two red lines.